

See discussions, stats, and author profiles for this publication at: <https://www.researchgate.net/publication/263946714>

Numerical Predictions of Momentum and Heat Transfer Characteristics from a Heated Sphere in Yield-Stress Fluids

ARTICLE in INDUSTRIAL & ENGINEERING CHEMISTRY RESEARCH · MAY 2013

Impact Factor: 2.59 · DOI: 10.1021/ie400703t

CITATIONS

16

READS

25

3 AUTHORS:



Neelkanth Nirmalkar
University of Birmingham

16 PUBLICATIONS 133 CITATIONS

[SEE PROFILE](#)



Raj Chhabra
Indian Institute of Technology Kanpur

222 PUBLICATIONS 3,991 CITATIONS

[SEE PROFILE](#)



Robert John Poole
University of Liverpool

93 PUBLICATIONS 956 CITATIONS

[SEE PROFILE](#)

Numerical Predictions of Momentum and Heat Transfer Characteristics from a Heated Sphere in Yield-Stress Fluids

N. Nirmalkar,[†] R. P. Chhabra,^{*,†} and R. J. Poole[‡]

[†]Department of Chemical Engineering, Indian Institute of Technology, Kanpur, India 208016

[‡]School of Engineering, University of Liverpool, Liverpool, L69 3GH, United Kingdom

ABSTRACT: In this work, momentum and heat transfer characteristics of a heated sphere immersed in visco-plastic media have been studied over a wide range of conditions: plastic Reynolds number, $1 \leq Re \leq 100$, Prandtl number, $1 \leq Pr \leq 100$, and Bingham number, $0 \leq Bn \leq 10^4$. The equations of motion and energy have been solved numerically to elucidate the influence of each of these dimensionless parameters on the local characteristics like streamlines, isotherms, kinematics of flow, local Nusselt number, etc. as well as on the gross engineering parameters such as drag coefficient and surface average Nusselt number. Furthermore, a detailed examination of the so-called yielded (fluid-like) and unyielded (solid-like) regions in the flow domain is carried out as a function of both the Reynolds and Bingham numbers. The present results have been compared with the scant results available in the literature and these are found to be in good agreement. Finally, the present numerical results for drag and Nusselt number (in the form of the so-called *j*-factor) have been correlated with the modified Bingham and Reynolds number via simple expressions thereby enabling their interpolation for the intermediate values of these dimensionless parameters.

1. INTRODUCTION

During the past 50 years or so, much has been written about the motion of a sphere in different types of non-Newtonian fluids.^{1–3} The interest in this flow configuration stems from both fundamental and pragmatic considerations. From a theoretical standpoint, the steady flow past a sphere constitutes a classical problem within the domain of transport phenomena. Also, this simple configuration which is free from geometric singularities has been used to test the applicability of the rheological parameters deduced from viscometric flows to a nonviscometric flow produced by a translating sphere.³ Similarly, this configuration has been also used to benchmark the performance of various numerical methodologies employed for computing visco-elastic flows.^{1,2} From a practical standpoint, reliable knowledge of the drag force experienced by a sphere falling through confined and unconfined fluids is also relevant for the stability of suspensions encountered in the food, pharmaceutical, and personal-care product sectors as well as in the process calculations while designing equipment for pipeline transportation, heating/cooling of slurries, gravity-based separation, etc.^{3–6} Consequently, over the years, a reasonable body of knowledge has accrued on various aspects of this problem including steady and transient behavior, wall effects, and detailed velocity fields, etc. as far as the visco-elastic and purely viscous (without yield stress) media are concerned. This information has been summarized among others by Tanner and Walters,¹ McKinley,² and Chhabra.³ An examination of the available literature clearly suggests that fluid mechanical aspects such as drag coefficient, wall effects, etc. have been investigated much more extensively than the corresponding heat/mass transfer aspects. Notwithstanding the early attempts at employing the standard boundary-layer approximations for power-law fluids due to Acrivos and co-workers,^{7,8} only recently have numerical results based on the solution of the complete forms of the momentum and energy

equations for a sphere in power-law fluids been reported. Thus, for instance, Dhole et al.⁹ were probably the first to report on the forced convection heat transfer from a heated unconfined sphere in power-law fluids. These results have been subsequently extended to a confined sphere^{5,6,10,11} exposed to uniform and Poiseuille-type fully developed profiles in tube flow of power-law fluids.^{10,11} The corresponding results in the free convection¹² and mixed-convection¹³ regimes from an isothermal sphere in power-law fluids have been reported very recently. Suffice it to say here that shear-thinning fluid behavior facilitates heat transfer, whereas shear-thickening behavior impedes it with reference to the trends in Newtonian fluids at fixed values of the governing parameters, that is, Reynolds number in the forced convection, Grashof number in the free convection, and Grashof and Richardson numbers in the mixed convection regimes. Also, the enhancement in heat transfer was significant only under conditions when advection was significant. However, the aforementioned studies are restricted to the so-called axisymmetric laminar flow regime only.

In contrast, many systems of industrial significance such as slurries, foams, or emulsions exhibit the so-called visco-plastic fluid behavior which is characterized by the existence of an apparent yield stress.^{14–16} Whether a true yield stress exists or not, the steady-shear behavior of many time-independent fluids is explained by postulating the existence of a yield stress in such structured fluids. Hence, such fluids can support weight of particles in unsheared conditions. This notion is used extensively in the formulation and manufacture of personal care and pharmaceutical products, cleaning aids, foodstuffs, etc., where it is of central importance to keep particles from settling

Received: March 4, 2013

Revised: April 22, 2013

Accepted: April 25, 2013

Published: April 25, 2013



under the influence of gravity.³ Aside from such overwhelming practical relevance, the motion of particles in yield stress fluids is also challenging from a computational viewpoint due to the discontinuity inherent in the commonly used viscosity models employed to approximate the rheological behavior of visco-plastic fluids. Thus, over the years, a few regularization techniques have evolved which smoothen the abrupt transition between yielded/unyielded parts of the flow domain; however, the two such regularization schemes which have gained wide acceptance are the so-called biviscous and the exponential regularization due to Papanastasiou.¹⁷ The relative merits and demerits of these two as well as that of the other techniques have been critically reviewed recently among others by Glowinski and Wachs.¹⁸ Admittedly, the first experimental study on the motion of spheres in Bingham fluids was reported almost 50 years ago,¹⁹ and many other experimental results have been reported since, (for example, see refs 20–26, etc). Most of the experimental studies have been thoroughly reviewed in ref 3. While the early experimental results^{19–21} leave a lot to be desired in terms of their precision, subsequent studies (e.g., see refs 22–26) have rectified most of the deficiencies in terms of fluid characterization and experimental protocols and therefore, the latter results have been shown to be reliable, but unfortunately these are limited to the so-called low Reynolds numbers (negligible inertial effects). On the other hand, the numerical studies are restricted to the so-called creeping-flow region (vanishingly small Reynolds number) only. Undoubtedly, Beris et al.²⁷ were the first to report on the creeping motion of a sphere in Bingham plastic fluids using a finite element method. They, however, employed the regularization proposed by Bercovier and Engelman²⁸ ($m = 10^5$) in the fluid-like (yielded) region in the vicinity of a sphere. Subsequently, these results have been verified by other studies.^{29–31} Also, these are in line with the currently available experimental results both in terms of the drag coefficient as well as the size and shape of the main yielded regions in the vicinity of the sphere. Excellent overviews, especially of the computational aspects of this problem, are provided by Putz et al.^{32,33} who have also reviewed the limited literature on hydrodynamic interactions between two spheres in visco-plastic fluids. The effects of particle shape and orientation on the drag behavior in such visco-plastic fluids with and without shear-thinning fluid behavior have been studied by Magnin and co-workers.^{34–36}

In summary, it is thus abundantly clear from the foregoing description that there are no numerical results available on the drag behavior of a spherical particle undergoing steady translation in visco-plastic fluids at finite Reynolds numbers, and to the best of our knowledge, no prior results exist on convective heat transfer from a heated sphere in visco-plastic media. This work endeavors to bridge this gap in the current literature. In particular, the governing equations (continuity, momentum, and energy) have been solved numerically for the following ranges of conditions: Reynolds number, $1 \leq Re \leq 100$, Prandtl number, $1 \leq Pr \leq 100$ and Bingham number, $0 \leq Bn \leq 10^4$.

2. PROBLEM FORMULATION AND GOVERNING EQUATIONS

Let us consider the axisymmetric, incompressible, steady flow of a visco-plastic fluid with a uniform velocity, V_0 , and at temperature, T_0 , over a heated sphere of diameter, d , as shown schematically in Figure 1. Since it is not possible to simulate numerically truly an unconfined flow, it is therefore customary

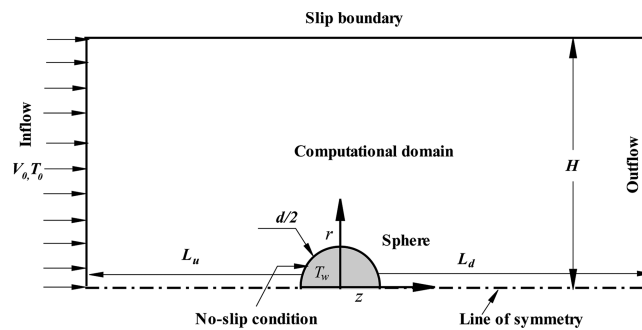


Figure 1. Schematic diagram of flow and of computational domain.

to introduce an artificial domain in the form of a cylinder and the sphere is situated at its axis. The surface of the sphere is maintained at a constant temperature, T_w , which is higher than that of free stream of the fluid, T_0 thereby resulting in convective heat transfer from the sphere to the ambient fluid or vice versa. To keep the level of complexity at a tractable level, the thermo-physical properties of the fluid (thermal conductivity, k , heat capacity, C , plastic viscosity, μ_B , yield stress, τ_0 , and density, ρ) are assumed to be temperature-independent. The viscous dissipation effect is also assumed to be negligible. While these assumptions lead to the decoupling of the velocity and temperature fields, at the same time, these also restrict the applicability of the present results to situations with small values of $\Delta T = T_w - T_0$ so that it is justified to neglect their variation with temperature. Within the framework of the aforementioned assumptions, the equations of continuity, momentum, and thermal energy (in their dimensionless form) can be written as follows:

Continuity equation:

$$\nabla \cdot V = 0 \quad (1)$$

Equation of motion:

$$(V \cdot \nabla)V = -\nabla p + \frac{1}{Re} \nabla \cdot \tau \quad (2)$$

Thermal energy equation:

$$(V \cdot \nabla)T = \frac{1}{Re Pr} \nabla^2 T \quad (3)$$

The deviatoric part of the stress tensor τ is given by the Bingham plastic constitutive relation which for a simple shear flow can be written as follows:

$$\tau = \left(1 + \frac{Bn}{|\dot{\gamma}|} \right) \dot{\gamma}, \quad \text{if } |\tau| > Bn \quad (4)$$

$$\dot{\gamma} = 0, \quad \text{if } |\tau| \leq Bn \quad (5)$$

In eq 4 and eq 5, $|\tau|$ and $|\dot{\gamma}|$ represent the magnitudes of the extra stress and the rate of deformation tensor, respectively. As noted earlier, the inherently discontinuous nature of the Bingham constitutive equation, eq (4) and eq (5), is not amenable to implementation in a numerical scheme for the solution of the field equations. Hence, to obviate this difficulty, a few regularization schemes have been proposed in the literature which effectively converts this discontinuity into a gradual transition between the fluid-like and solid like regions prevailing in the flow field. For instance, Papanastasiou¹⁷ proposed a modified model with a growth rate parameter (m) which provides not only a smooth transition from solid-like

region to liquid-like region, but also reduces the possible oscillations in achieving the prechosen level of convergence of the numerical solution. In this approach, the modified Bingham plastic model is rewritten as follows:

$$\tau = \left(1 + \frac{Bn[1 - \exp(-m|\dot{\gamma}|)]}{|\dot{\gamma}|} \right) \dot{\gamma} \quad (6)$$

Evidently, at large values of the growth rate parameter, m , eq 6 approaches the original Bingham plastic model, though very large values of m can also lead to numerical instabilities. Therefore, care is needed in choosing an appropriate value of m in a given situation. The other approaches used in circumventing the discontinuous nature of the yield stress fluid models together with their merits and demerits have been reviewed by a few workers, for example, see Liu et al.,³⁷ Frigaard and Nouar,³⁸ Glowinski and Wachs,¹⁸ Bercovier and Engleman,²⁸ Donovan and Tanner,³⁹ etc.

For incompressible fluids, the deviatoric stress tensor can be written as follows:

$$\tau = \eta \dot{\gamma} \quad (7)$$

and thus for a Bingham plastic fluid, the scalar viscosity η is given as

$$\eta = \left(1 + \frac{Bn[1 - \exp(-m|\dot{\gamma}|)]}{|\dot{\gamma}|} \right) \quad (8)$$

where $\dot{\gamma}$ is the rate-of-strain tensor which is given by

$$\dot{\gamma} = (\nabla V + \nabla V^T) \quad (9)$$

The magnitudes of the rate of deformation tensor and deviatoric stress tensor are given by

$$|\dot{\gamma}| = \sqrt{\frac{1}{2} \text{tr}(\dot{\gamma}^2)} \quad (10)$$

$$|\tau| = \sqrt{\frac{1}{2} \text{tr}(\tau^2)} \quad (11)$$

The aforementioned governing equations are rendered dimensionless using d , V_0 , and $\mu_B(V_0/d)$ as scaling variables for length, velocity, and stress components, respectively. The temperature and regularization parameter, m , were rendered dimensionless as $T = (T' - T_0)/((T_w - T_0))$ and (V_0/d) , respectively. Thus, the momentum and forced convection heat transfer characteristics in the present case are governed by three dimensionless parameters, namely, Bingham number (Bn), Reynolds number (Re), and Prandtl number (Pr), which are defined as follows:

$$Bn = \frac{\tau_0 d}{\mu_B V_0} \quad (12)$$

The two limiting conditions of the Newtonian fluid and of the fully plastic behavior correspond to $Bn \rightarrow 0$ and $Bn \rightarrow \infty$, respectively.

$$Re = \frac{\rho d V_0}{\mu_B} \quad (13)$$

$$Pr = \frac{C \mu_B}{k} \quad (14)$$

At this juncture, it is worthwhile to remark here that the preceding definitions of the Reynolds number and Prandtl

number are based on the constant values of μ_B and τ_0 appearing in the Bingham plastic model, eq 4. However, if one were to define these parameters based on the effective viscosity evaluated at the characteristic shear rate of (V_0/d) , one can easily show that it would lead to the following modified definitions of the Reynolds number, Re^* , Prandtl number, Pr^* , and Bingham number, Bn^* :

$$Re^* = \frac{Re}{(1 + Bn)} \quad (15)$$

$$Pr^* = Pr(1 + Bn) \quad (16)$$

$$Bn^* = \frac{Bn}{(1 + Bn)} \quad (17)$$

Indeed, these modified definitions were found to be more effective in correlating the drag and Nusselt number results for the transverse flow of Bingham plastic fluids past a long bar of square cross section⁴⁰ and earlier for drag on a sphere.^{20–23}

The problem definition is completed by prescribing the following (dimensionless) boundary conditions. On the surface of the sphere, the usual no-slip and impenetrability ($V_r = 0$; $V_z = 0$) condition and constant temperature ($T = 1$) are used. At the inlet of the tubular domain, uniform flow in the z -direction ($V_z = 1$; $V_r = 0$) and free stream fluid temperature ($T = 0$) are used. The fictitious walls of the tubular domain are treated as tractionless and adiabatic; that is, $\partial V_z / \partial r = 0$, $V_r = 0$ and $\partial T / \partial r = 0$ are implemented here. Likewise, these conditions are also prescribed on the plane of symmetry. Lastly, at the exit of the tube, the flow is assumed to be fully developed, that is, $\partial \varphi / \partial z = 0$ is used for all dependent variables except for pressure. However, the gradients can still exist in the r -direction at the exit plane. Once the flow domain is mapped in terms of the primitive variables ($u-v-p-T$), these can be postprocessed to evaluate the local and global kinematic and thermal parameters of interest.

At this juncture, it is thus appropriate to introduce definitions of some of the integral parameters such as drag coefficient and Nusselt number which will be used extensively in the subsequent discussion:

Drag Coefficient (C_D). This is a measure of the hydrodynamic force exerted by the fluid on the submerged sphere in the direction of flow. The drag force is made up of two components, namely, shearing forces (C_{DF}) due to friction and normal forces (C_{DP}). These are defined as follows:

$$C_{DF} = \frac{2F_{DF}}{\rho V_0^2 \left(\frac{\pi}{4} d^2 \right)} = \frac{2}{Re} \int_s \tau \cdot n_s \, ds \quad (18)$$

$$C_{DP} = \frac{2F_{DP}}{\rho V_0^2 \left(\frac{\pi}{4} d^2 \right)} = \frac{2}{Re} \int_s C_p n_z \, ds \quad (19)$$

$$C_D = C_{DF} + C_{DP} \quad (20)$$

where C_p is the pressure coefficient defined as

$$C_p = \frac{P_0 - P_\infty}{\frac{1}{2} \rho V_0^2} \quad (21)$$

In eq 21, P_0 is the local pressure at a point on the surface of the sphere which varies along the surface of the sphere, and P_∞ is its reference value far away from the sphere. Naturally, eq 21 leads to a family of curves corresponding to different values of

Bingham number and Reynolds number. On the other hand, it is possible to consolidate the present numerical results by introducing a modified pressure coefficient where the pressure is scaled by the yield stress ($C_p^* = C_p \times Re^*$)

Nusselt Number (Nu). This gives the nondimensional rate of heat transfer between the fluid and sphere or vice versa. By equating the heat flux by conduction and convection at a point on the surface of the sphere, it can easily be shown that the local Nusselt number is given by

$$Nu = \frac{hd}{k} = -\frac{\partial T}{\partial n_s} \quad (22)$$

Where n_s is the outward drawn unit normal vector on the surface of the sphere. From a practical standpoint, the overall mean value of the Nusselt number is frequently required in process design calculations to estimate the rate of heat loss (or gain) from the sphere, if the two temperatures are known, or one of the unknown temperatures, if the heat flux is known from heat duty considerations. The surface averaged value is obtained by simply integrating the local values of the Nusselt number over the surface of the sphere as

$$Nu_{avg} = \frac{1}{S} \int_S Nu \, dS \quad (23)$$

Notwithstanding the significance of the detailed structure of the velocity and temperature fields, yielded/unyielded surfaces which provide useful insights about the well-mixed or poorly mixed pockets of the fluid, the gross characteristics of drag coefficient and the average Nusselt number are expected to be functions of Reynolds number, Bingham number, and Prandtl number. This work endeavors to explore and develop an understanding of this functional dependence.

3. NUMERICAL SOLUTION METHODOLOGY AND CHOICE OF NUMERICAL PARAMETERS

In this study, the aforementioned governing equations subject to the foregoing boundary conditions together with the constitutive relation have been solved numerically using the finite element based solver Comsol Multiphysics (version 4.2). A quadrilateral mesh has been used to solve the discretized forms of governing equations in terms of the primitive variables, that is, velocity, pressure, and temperature. As noted earlier, at high values of the Reynolds number, Prandtl number, and Bingham number, the velocity and temperature gradients are expected to be very steep particularly in the vicinity of the heated sphere and near the interface between the fluid-like and solid-like regions due to very thin boundary layers and hence a relatively fine mesh has been used in these regions. Furthermore, the regularized-viscosity approach of Papanastasiou¹⁷ is introduced here in the form of a user defined function. The solution was always initiated using the converged Newtonian flow field to avoid the potential convergence difficulties reported in such situations. A relative convergence criterion of 10^{-7} for the equations of momentum and energy has been used in this work.

Much has been written in our recent studies on yield stress fluids^{40,42,43} about the influence of numerical aspects on the results, and therefore, a judicious choice of the computational domain (values of L_u , L_d , and H) and mesh, and of the regularization parameter (m) is germane to obtain results free from such numerical artifacts. For this purpose, the values of each of the domain parameters were systematically varied as: L_u

= 20d, 30d, 40d, L_d = 10d, 20d, 30d and H = 20d, 30d, and 40d for the lowest values of $Re = 1$, $Pr = 1$, and $Bn = 0$ (Newtonian fluid behavior); Table 1 presents a summary of results

Table 1. Domain Independence Studies at $Re = 1$, $Pr = 1$, and $Bn = 0$

influence of upstream length			
L_u	C_{DP}	C_D	Nu_{avg}
10	9.745	28.321	2.5214
20	9.128	27.634	2.3244
30	9.112	27.623	2.3214
influence of downstream length			
L_d	C_{DP}	C_D	Nu_{avg}
10	9.524	27.965	2.7541
30	9.128	27.634	2.3244
40	9.102	27.633	2.3192
influence of lateral length			
H	C_{DP}	C_D	Nu_{avg}
20	9.624	28.512	2.3541
30	9.128	27.634	2.3244
40	9.115	27.610	2.3195

elucidating the effect of each of these parameters. An examination of these results clearly suggests that the present numerical results (pressure and total drag coefficient, Nusselt number), obtained with the largest value of L_u , L_d , and H tested here, change very little, albeit the corresponding CPU time increased several fold. Therefore, the values $L_u = 20d$, $L_d = 30d$, and $H = 30d$ denote an acceptable compromise between the precision of the results and the computational cost. Since the velocity and temperature gradients are expected to be very steep at large values of Re , Pr , and Bn , Table 2 shows the effect of computational mesh on the drag and Nusselt number values at the maximum values of these parameters; the values obtained with mesh G2 and G3 are seen to be virtually indistinguishable from each other and therefore, the new results reported herein have been obtained with G2. Finally, the influence of the value of the regularization parameter, m , on the numerical results is summarized in Table 3, and its influence on the location of the yield surfaces is shown in Figure 2. Once again an inspection of Table 3 indicates $m = 10^6$ is adequate to obtain reliable results. On the other hand, Figure 2 shows that the shape of the faraway yield surface is slightly sensitive to the value of m . Notwithstanding the fact that the values of drag coefficients and Nusselt number are determined primarily by the gradients (velocity and temperature) on the surface of the sphere, the minor influence of the value of m seen faraway from the sphere is of little relevance here. On this count also, the value of $m = 10^6$ is considered to be adequate for the range of conditions embraced here. The selection of these parameters is further substantiated by presenting a few benchmark comparisons in the next section.

4. RESULTS AND DISCUSSION

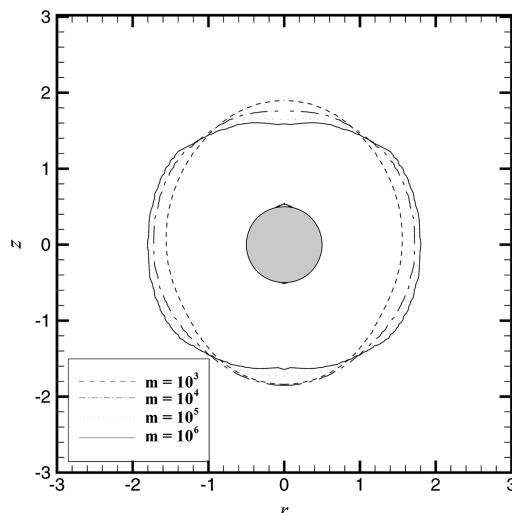
In this work, the momentum and forced convection heat transfer characteristics of an isothermal sphere have been considered at finite Reynolds numbers over wide ranges of the pertinent parameters as follows: $1 \leq Re \leq 100$; $1 \leq Pr \leq 100$; and $0 \leq Bn \leq 10^4$. In particular, the effect of each of these parameters on the detailed velocity and temperature profiles, the size and shape of yielded-regions, drag, and Nusselt number

Table 2. Effect of Grid Size on the Present Results

$Re = 100, Pr = 100$							
grid	elements	C_D		C_{DP}		Nu_{avg}	
		$Bn = 0$	$Bn = 10^4$	$Bn = 0$	$Bn = 10^4$	$Bn = 0$	$Bn = 10^4$
G1	7021	1.124	2895.1	0.5214	2189.5	33.965	84.475
G2	10141	1.096	2885.4	0.5119	2185.2	33.579	84.453
G3	15322	1.091	2881.1	0.5091	2184.6	33.551	84.412

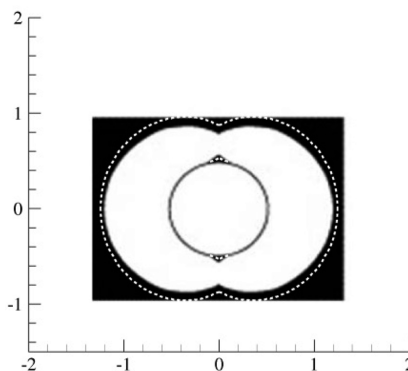
Table 3. Influence of Growth Rate Parameter on the Results at $Re = 50$ and $Pr = 1$

m	$Bn = 10$		$Bn = 10^4$	
	C_D	Nu_{avg}	C_D	Nu_{avg}
10^4	8.8671	3.3449	5762.76	3.8712
10^5	9.0597	3.4271	5769.57	3.9501
10^6	9.0883	3.4403	5770.63	3.9614
10^7	9.0933	3.4425	5770.97	3.9636

Figure 2. Influence of regularization parameter, m , in the Papanastasiou model on yield surface at $Re = 50$ and $Bn = 10$.

have been elucidated. However, prior to undertaking a detailed discussion of the new results, it is desirable to establish the accuracy and reliability of the numerics used in this work.

4.1. Validation of Results. To demonstrate that the present numerical results are free from numerical artifacts, a few benchmark comparisons are presented here. Mitsoulis and Zisis⁴¹ have reported reliable numerical results on the flow of a Bingham plastic fluid in a lid-driven square cavity. Suffice it to say here that the present predictions of the unyielded/yielded regions were found to be in excellent agreement with that of Mitsoulis and Zisis,⁴¹ except for the fact that their predictions of the interface were not very smooth due to the relatively coarse mesh and the small value of $m = 10^4$ used in their study as opposed to the value of $m = 10^6$ used in the present case. Next, Figure 3 compares the yielded/unyielded regions as predicted in this work with that of Beris et al.²⁷ and once again, the two predictions are seen to be in good agreement with each other. It is worthwhile to comment here that the black material is moving but as a solid plug (i.e., the velocity gradient in this region is essentially zero) whereas the white material is truly flowing. An imperfect analogy to understand what Figure 3 is showing is to think of the black-white interface as something akin to the material "melting" upstream and "freezing"

Figure 3. Comparison of present unyielded/yielded regions (broken line) in creeping flow regime at Bingham number, $Bn = 544.7$ with that of Beris et al.²⁷ (Flow is from bottom to top.)

downstream at the white-black interface. Furthermore, the present values of the Stokes' drag coefficient ($C_s = F_D / (6\pi\mu_B V_0 R)$) are also compared with that of Beris et al.²⁷ and Liu et al.³⁶ as shown in Table 4. The present results are seen to

Table 4. Comparison of the Present Values of the Stokes Drag Coefficient with the Literature Values

Bn	C_s		
	Beris et al. ²⁷	Liu et al. ³⁶	present
8.047	15.21	15.24	15.25
59.59	82.77	82.67	82.83
340.7	426.9	426.0	427.5
544.6	669.7	671.9	673.5

be virtually indistinguishable from that of Beris et al.²⁷ and Liu et al.³⁶ Finally, unfortunately, no prior results are available on heat transfer from a sphere in Bingham plastic fluids. However, in the limit of Newtonian fluid behavior, that is, $Bn = 0$, the present values of the average Nusselt number were found to be within 1% of the values reported recently^{10,11} (Table 5). On the basis of these comparisons and those reported in our recent studies,^{40,42,43} the new results obtained in this work are regarded to be reliable within ca. 1.5–2%.

4.2. Streamline contours. Representative streamline contours are shown in Figure 4 for scores of values of the Bingham number and Reynolds number. Broadly, the inertial forces (increasing Reynolds number) tends to the occurrence of the so-called adverse pressure gradient in the rear of the sphere which results in the detachment of flow from the surface of the sphere, eventually resulting in the formation of twin symmetric (counter rotating) vortices. The presence of the yield stress however acts to stabilize the flow, that is, the propensity for flow separation is suppressed. Thus, for instance, in Newtonian fluids ($Bn = 0$), the flow separates from the surface of the sphere at about $Re \approx 22$ –24. Of course, well-

Table 5. Comparison of the Present Results with the Literature Values

<i>Re</i>	<i>Pr</i>	<i>Nu</i> _{avg}		
		Dhole et al. ¹⁹	Song et al. ²⁰	present
5	1	3.032	3.025	3.026
	5	4.326	4.314	4.315
	50	8.077	8.026	8.037
	100	9.930	9.802	9.861
50	1	5.963	5.963	5.964
	5	9.505	9.498	9.511
	10	11.707	11.636	11.717
	20	14.478	14.168	14.502
100	1	7.749	7.683	7.6847
	5	12.895	12.551	12.640
	10	16.21	15.376	15.753
	20	20.429	18.487	19.680

developed wake regions are formed at $Re = 50$ and $Re = 100$. The present values of the wake lengths for ($Bn = 0$) are in line with the scant experimental results available in the literature.^{44–46} On the other hand, the introduction of yield stress, howsoever small, clearly suppresses the tendency for flow separation. Thus, the flow remains attached even up to $Re = 100$ with as small a value of the yield stress as $Bn = 1$. This behavior is qualitatively consistent with the findings of Mossaz et al.⁴⁷ for a circular cylinder.

4.3. Yielded/Unyielded zones. Since one of the distinguishing features of yield-stress fluids is the simultaneous presence of yielded and unyielded regions in the flow domain, it is thus customary to examine the influence of Bingham and Reynolds numbers on the size and shape of the yielded regions. Figure 6 shows representative results on this aspect. The creeping flow results shown in Figure 4 confirmed the symmetric nature of the flow field about both the *r*-axis and *z*-axis. This trend continues broadly at a gross level at high Reynolds number also, albeit the flow field is not expected to show complete fore-and aft-symmetry in the presence of inertial effects. In the limit of Newtonian fluid behavior ($Bn = 0$), the momentum boundary layer progressively thins with increasing Reynolds number and therefore shearing of the fluid is confined to this thin layer. The introduction of yield stress accentuates this tendency. On both counts, the size of the yielded region gradually shrinks and it is mainly situated adjacent to the sphere. The two polar caps denoting the unyielded material seen in Figure 2 at zero Reynolds number are still present at finite Reynolds number. In addition to Papanastasiou's regularization, a few simulations were performed using the biviscosity model (with $\mu_y/\mu_B \leq 10^6$) in order to corroborate the foregoing trends of the present results. However, the results changed very little for the value of this ratio above 10^4 and therefore, most of the results are based on the choice of ($\mu_y/\mu_B = 10^4$). The resulting yield surface is shown as dotted lines in Figure 5. While the shape of the yield surface predicted by the both regularization schemes is seen to be qualitatively similar, the biviscous model seems to predict a slightly larger fluid-like cavity than the exponential regularization of Papanastasiou. On the other hand, such minor discrepancies are probably of not much significance as far as the values of the drag coefficient and Nusselt number are concerned which are mainly determined by the velocity and temperature gradients on the surface of the sphere (Table 6). This convergence of drag and Nusselt number data using both

regularizations also demonstrates that it is possible to use either of these schemes as long as prudent values of the numerical parameters are selected, that is, the value of *m* or of the ratio of the yielding to Bingham viscosity. In summary, the fluid-like zone is seen to shrink with increasing Bingham number.

4.4. Flow Kinematics. Figures 6 and 7 show the axial velocity profiles along the *z*- and *r*-axes at Reynolds numbers of $Re = 1$ and 100 for different values of the Bingham number. An inspection of Figure 6 shows that there are four different segments of the curve at high Bingham numbers, namely, segment *ab*, *bc*, *cd*, and *de*. For a Bingham plastic fluid, the segment *ab* represents the region of sudden change in velocity, that is, the region of high velocity gradient. In segment *bc*, the change in velocity is not only less steep (as can be gauged from the slope of *bc*) but also the change itself is also smaller in magnitude. Next, the segment *cd* exhibits negative slope corresponding to a fluid-like region with a very high strain rate, and segment *de* shows the outer envelope translating with constant free stream velocity like a rigid mass of fluid. Hence, there are three distinct zones with high strain rates adjacent to each other. Similarly, an examination of the velocity profiles along the *z*-direction (Figure 7) shows three different segments irrespective of the value of the Bingham number including the case of $Bn = 0$ namely, segment *ab*, *bc*, and *cd*. Here, the segment *ab* represents a polar cap attached to the sphere in case of Bingham plastic fluids, whereas it corresponds to the wake region with twin vortices attached to the rear surface of a sphere in Newtonian fluids. Similarly, the segment *bc* indicates the flow region with very high shear rates both in Bingham and Newtonian fluids and finally, the segment *cd* shows the dynamic envelope of the unyielded region in Bingham fluids. In summary, there is only one segment with high shear rate in this direction which is situated in between the polar caps and the outer unyielded envelope. While it is not possible to make detailed comparisons with the experimental results of Attapattu et al.,^{22,23} suffice it to say here that the trends seen in Figures 6 and 7 are in line with their observations.

Some further insights can be gained by examining the velocity and shear rate contour plots as shown in Figure 8. As noted earlier, owing to the presence of yield stress, yielded (fluid-like) zones are always located close to the sphere, and this is seen as the relatively large value of velocity in the vicinity of sphere. Similar trends are revealed by shear rate contours as shown in Figure 8b. Finally, the rate of deformation in Bingham fluids in the vicinity of the sphere is seen to be higher than that in a Newtonian fluid otherwise under identical conditions. At the next level, it is customary to analyze the pressure variation along the surface of the sphere. Figure 9 shows representative results on the variation of pressure coefficient along the surface of sphere scaled by the modified Reynolds number. All else being equal, for Bingham plastic fluids, the surface pressure on the sphere is seen to be higher than that in Newtonian fluids. When plotted in this manner, the collapse of the data for all nonzero Bingham numbers shows that the pressure and yield stress are essentially in balance. Although not shown here, when the classical pressure coefficient data are plotted (i.e., normalized by the dynamic pressure $1/2\rho V^2$) the data appear to show a monotonic increase of the pressure with Bingham number purely as a consequence of the scaling used.

4.5. Drag coefficients. Because of the prevailing normal and tangential stresses on the surface of sphere, the fluid exerts a net hydrodynamic drag force (on sphere) made up of form, C_{DP} (due to pressure) and friction components, C_{DF} , and the

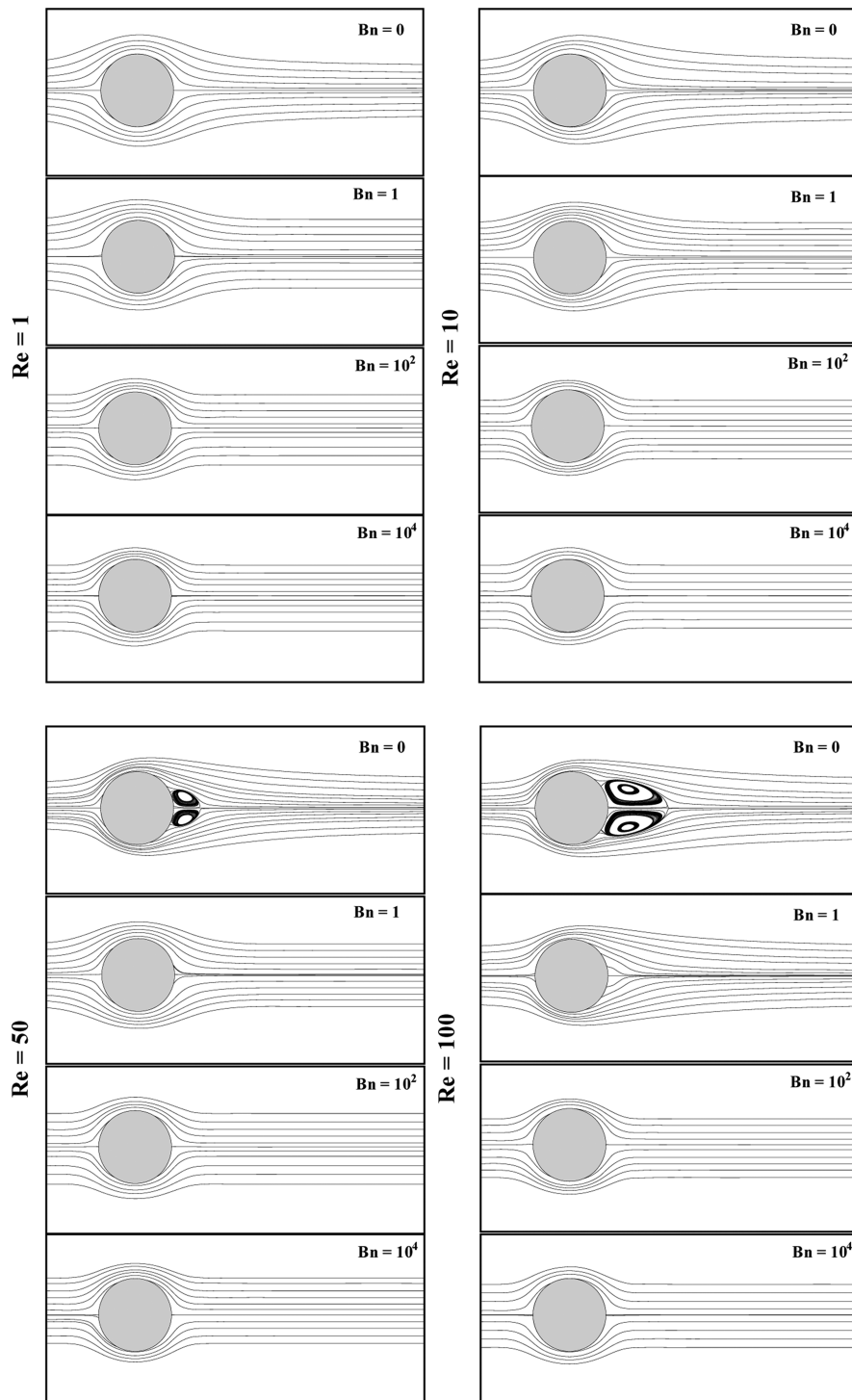


Figure 4. Representative streamline contours (flow is from left to right).

sum of these two is the total drag, eq 18–20. Naturally, in the present case when there is no coupling between the velocity and temperature fields, the two drag components are expected to be functions of the Reynolds and Bingham numbers. Undoubtedly, this approach yields a family of C_D – Re curves corresponding to each value of the Bingham number. However, it is possible that the modified definition of the Reynolds number, Re^* , and Bingham number, Bn^* , might consolidate the results for different values of the Bingham number thereby eliminating it from the set of dimensionless parameters. Indeed this approach was proposed by Ansley and Smith²⁰ almost 50

years ago, and has been used successfully subsequently in the literature^{22,23} for spheres, and recently for a square cylinder.⁴⁰ Therefore, it will be used here also. Figure 10 shows the functional relationship for both the pressure and total drag components. This is a classical inverse dependence of the drag coefficient on the Reynolds number. However, the values of $(C_{DP} \times Re^*)$ and $(C_D \times Re^*)$ are reasonably constant up to about $Re^* \approx 1\text{--}2$ beyond which the functional dependence is characterized by the decreasing slope of the C_D – Re^* curve, akin to that for Newtonian fluids. The present numerical results

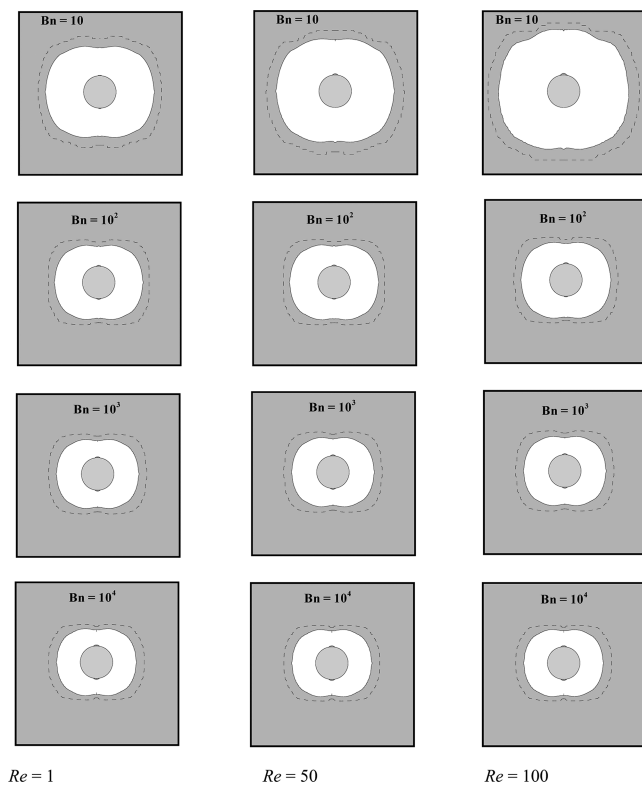


Figure 5. Influence of Bingham number on the yielded/unyielded regions predicted from Papanastasiou ($m = 10^5$) and biviscous model (broken line) ($\mu_y/\mu_B = 10^5$) (flow is from bottom to top).

(150 data points) are best approximated by the following functional relationships:

$$C_D \text{ or } C_{DP} = \frac{a}{Re^*} (1 + b Re^{*C}) \quad (24)$$

The resulting best values of these constants together with the corresponding mean and maximum deviations are summarized in Table 7. Finally, it is worthwhile to make a comparison between the present predictions and the scant experimental results available in the literature.^{19–23} To the best of our knowledge, only three independent data sets are available for drag on a sphere at finite Reynolds numbers.^{19–21} Figure 11 shows such a comparison where the correspondence is seen to be fair. However, in assessing this comparison, at least two factors must be borne in mind: first, such experiments are always conducted in finite sized tubes, and therefore the data always entail, howsoever small, wall effects. Second, both Valentik and Whitmore¹⁹ and Pazwash and Robertson²¹ evaluated the Bingham yield stress (τ_0) from their shear stress-shear rate data by extrapolating their flow curves to zero-shear rates. It is readily acknowledge that the resulting values of τ_0 are strongly dependent on the range of shear-rates spanned by the flow curve.^{3,48} On the other hand, Ansley and Smith²⁰ used the local slope of the flow curve corresponding to the shear rate of (V_0/d). The resulting values of Reynolds number and Bingham number are thus somewhere in between the Re/Re^* and Bn/Bn^* in the present context. In view of the foregoing factors, the correspondence between the predictions and observations shown in Figure 11 is regarded to be satisfactory and acceptable.

4.6. Isotherm Contours. Naturally, the temperature field prevailing in the vicinity of the heated sphere is directly

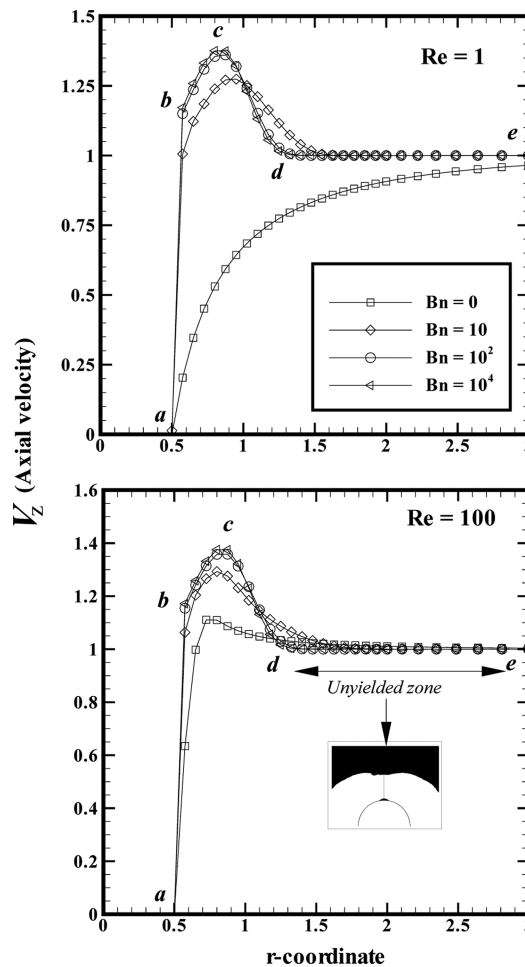


Figure 6. Axial velocity profile along line $z = 0$ at $Re = 1$ and 100 .

Table 6. Comparison of the Present Drag Results Predicted Using the Papanastasiou's Model and the Bi-Viscosity Model at $Bn = 10$

Re	Papanastasiou's model	biviscosity model
1	437.67	452.17
10	43.874	45.311
50	9.0917	9.3603
100	4.7701	4.8958

influenced by the corresponding velocity field. Obviously, in the so-called yielded regions, convection dominates the rate of heat transfer. In contrast, in the solid-like unyielded regions, heat transfer occurs primarily by conduction if this is a static region, whereas the conduction contribution is somewhat augmented by convection due to the rigid-body like motion, as were seen in Figure 9b. Thus, isotherm patterns follow closely the streamline patterns, especially for $Bn = 0$. Typical isotherm contours are plotted in Figures 12 and 13 for a range of combinations of the values of Pr and Bn for two extreme values of the Reynolds number. At low Peclet numbers ($Re \cdot Pr$), advection is weak and therefore the conduction mechanism dominates and the isotherms are seen to be more or less concentric circles, at least in the front half of the sphere. At $Pe = 1$, as the value of the Bingham number is progressively increased from $Bn = 0$ to $Bn = 10^4$, the isotherms cluster close to the surface of the sphere due to the shrinking yielded regions thereby resulting in high velocity and temperature gradients in

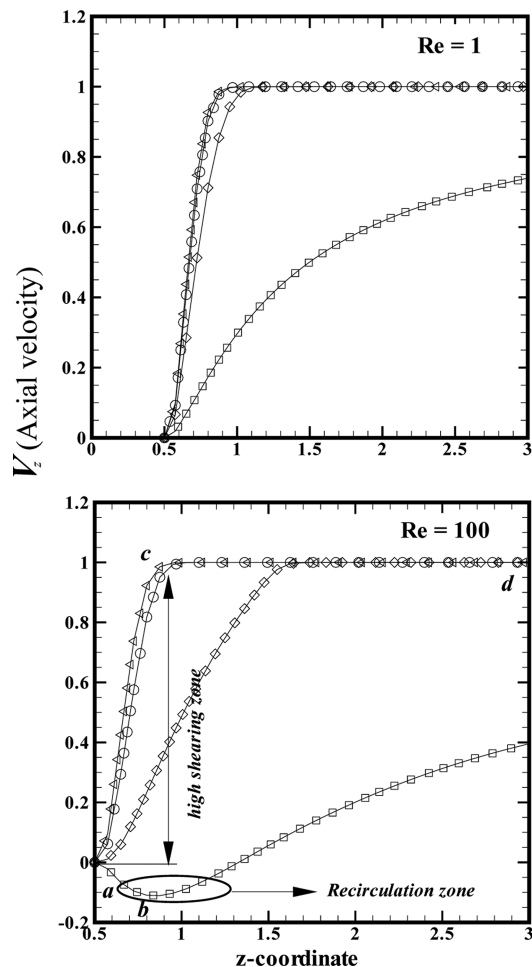


Figure 7. Axial velocity profile along line $r = 0$ and $z > 0$ at $Re = 1$ and 100. The segments ab , bc , cd , etc. denote the fluid in different kinematic states.

the thin fluid-like region. As the value of the Prandtl number is progressively increased, at a fixed Reynolds number, $Re = 1$, to $Re = 100$, further thinning of the thermal boundary layer is evident thereby suggesting a positive dependence of the rate of heat transfer (Nusselt number) on the Prandtl number. On the other hand, the effect of Reynolds number is seen to be much more dramatic in Figure 13. This is consistent with the fact that the boundary-layer thickness shows a stronger dependence on the Reynolds number than that on the Prandtl number. All in all, it is thus reasonable to anticipate a positive dependence of the Nusselt number on the Reynolds, Prandtl, and Bingham numbers. Indeed, this hypothesis is borne out by the Nusselt number results shown in the ensuing sections.

4.7. Local Nusselt Number Variation on the Surface of Sphere. At the outset, it is worthwhile to recognize here that the local value of the Nusselt number is given by the corresponding temperature gradient normal to the surface of the sphere. At the same time, the local fluid viscosity is also determined by the corresponding effective shear rate at that point. This implies that while the temperature along an isotherm contour remains constant, each point on the isotherm corresponds to a different fluid viscosity and hence continuously varying values of the local Reynolds number (Re), Prandtl number (Pr), and Bingham number (Bn). This is of no consequence in the case of Newtonian fluids where the fluid viscosity is independent of shear rate. However, this aspect

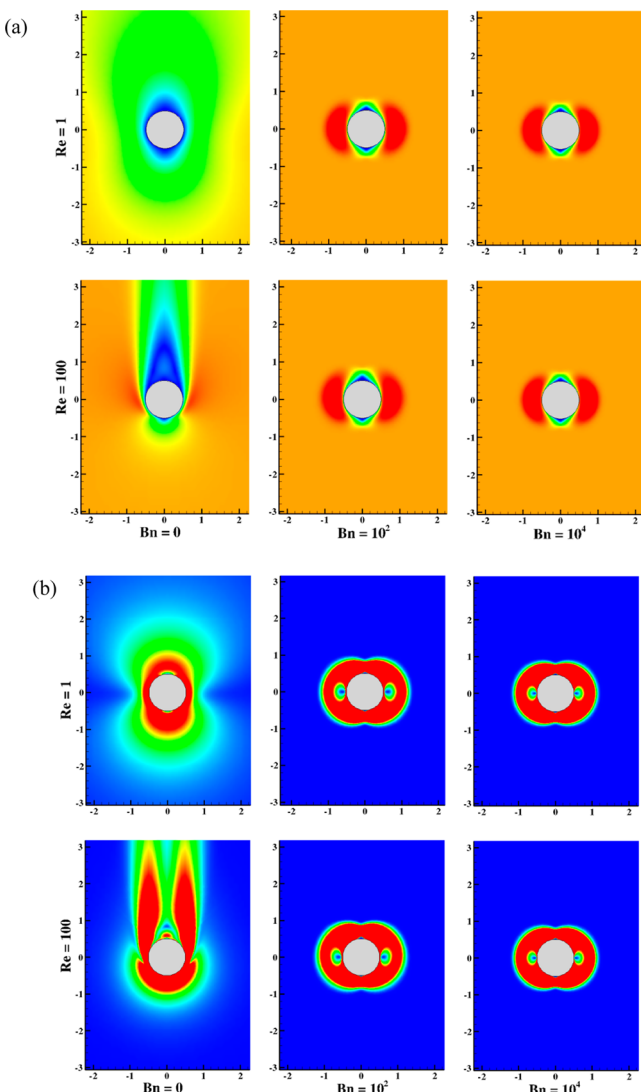


Figure 8. Contour diagram: (a) velocity magnitude; (b) shear rate magnitude.

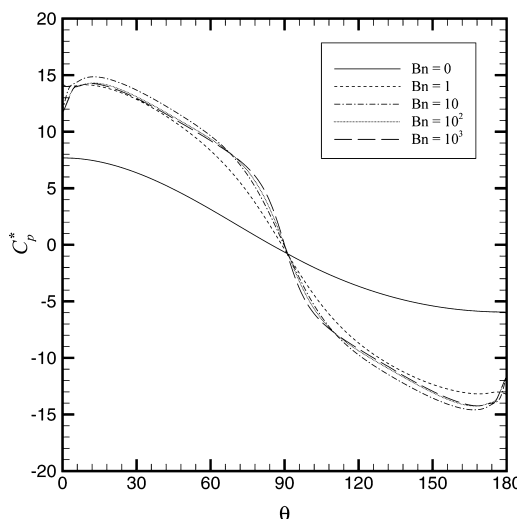


Figure 9. Variation of modified pressure coefficient, C_p^* along the surface of sphere (where $\theta = 0$ corresponds to the front stagnation point).

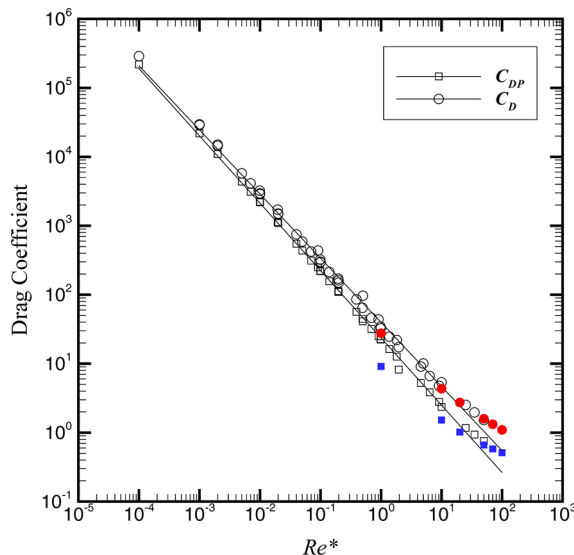


Figure 10. Influence of the modified Reynolds number on the total and pressure drag coefficients (filled color symbols represent Newtonian results).

Table 7. Values of Constants in eq 24.

	a	b	c	% error	
				mean	maximum
C _D	28.63	0.19	0.33	1.95	10.2
C _D (<i>Bn</i> = 0)	24.00	0.15	0.69	0.22	0.51
C _{DP}	21.84	0.04	0.77	2.65	12.7
C _{DP} (<i>Bn</i> = 0)	7.88	0.16	0.77	0.18	0.46

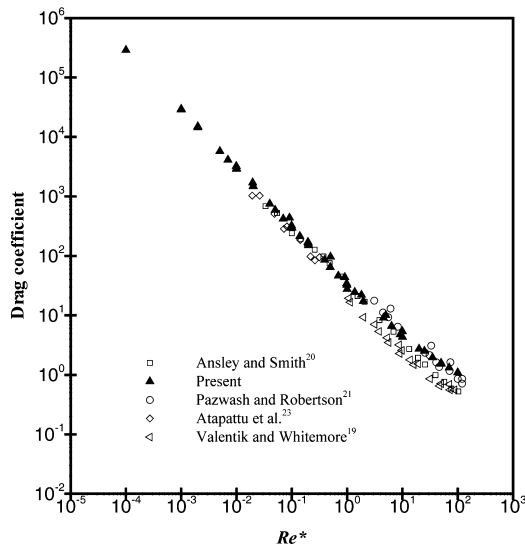


Figure 11. Comparison of the present drag results with the literature values.

adds to the complexity of the influence of *Bn*, *Re*, and *Pr* on heat transfer in the case of Bingham plastic fluids. Figure 14 shows a typical distribution of the local Nusselt number on the surface of the heated sphere for a range of values of the Prandtl number and Bingham numbers for the maximum value of the Reynolds number, namely, *Re* = 100.

It is useful to recall here that in Newtonian fluids (*Bn* = 0), the local Nusselt number decreases from its maximum value at the front stagnation point to its minimum value at the rear

stagnation point, at low Reynolds numbers where the flow remains attached (Figure 4 at *Re* = 1) and of course, the minimum Nusselt number occurs at the point of separation ($\theta \approx 128^\circ$) at *Re* = 100. Because of fluid circulation, it increases beyond the separation point. At low Peclet numbers, the Nusselt number was seen to change very little over the entire surface due to negligible convection under these conditions.

On the other hand, even at as small values of Bingham number as *Bn* = 1, some enhancement in heat transfer was evident in heat transfer over the bulk of the sphere surface even at *Re* = 1. This is simply attributed to the fact that the temperature field shows a rather faster spatial decay in a Bingham fluid than that in a Newtonian fluid. As the value of the Bingham number is progressively increased, the other unyielded regions begin to form which further influence the rate of heat transfer. Furthermore, the nature of the Nusselt number distribution is increasingly distorted from that seen at low values of Bingham number.

Since at *Re* = 1, the fluid inertia is still expected to be essentially negligible, this distortion must be solely due to the yield stress effects. One would eventually expect to see a limiting value of the Bingham number beyond which the role of Bingham number will be negligible. Of course, this limiting value will be a function of both *Pr* and *Re*. As the fluid inertia increases at *Re* = 100 (Figure 4), the effect of Bingham number is seen to be even more dramatic. First, since no recirculation region is formed at this Reynolds number, the Nusselt number continually decreases from the front stagnation point to the rear stagnation point. However, in this case, the maximum Nusselt number does not occur at the front stagnation point, and this is similar to that seen for heat transfer from an isothermal sphere in power-law fluids in all regimes, that is, forced,⁹ free,¹² and mixed-convection¹³ regimes. This effect can safely be attributed to the different rates of thinning of the momentum and thermal-boundary layers with *Re*, *Bn*, and *Pr*. In overall terms, the Nusselt number values are seen to increase with the increasing Reynolds number, Prandtl number, and Bingham number.

4.8. Average Nusselt Number. While isotherm contours and the local Nusselt number distribution are useful in delineating the locally “cold” or “hot” regions which might be relevant in the heating/cooling of temperature-sensitive products, reliable values of the surface average Nusselt number, Nu_{avg} , are often required in the sizing of process equipment in engineering applications. Dimensional considerations suggest the average Nusselt number Nu_{avg} to be a function of the pertinent parameters as

$$Nu_{avg} = f(Re, Pr, Bn) \quad (25)$$

By employing the modified definition of the Reynolds and Prandtl numbers, eq 25 can be recast in the following form:

$$Nu_{avg} = f(Re^*, Pr^*) \quad (26)$$

This still leads to a family of curves in Nu_{avg} - Re^* space for different values of the modified Prandtl number, Pr^* . Further consolidation of the numerical data was achieved by introducing the usual Colburn j_H factor defied as

$$j_H = \frac{Nu_{avg}}{Re^* Pr^{*1/3}} = f(Re^*) \quad (27)$$

Figure 15 shows the present heat transfer results, and the best fit is given by the equations,

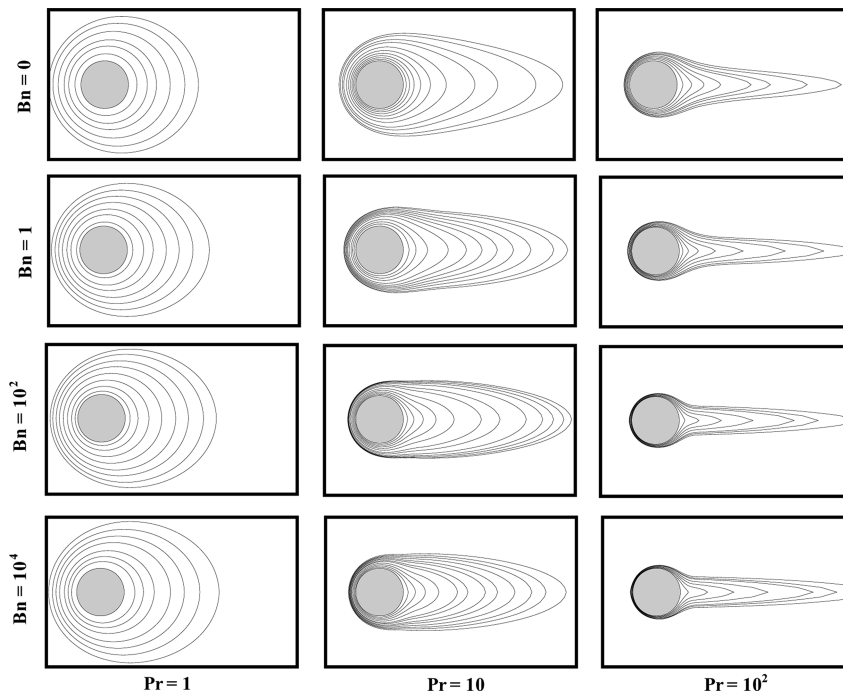


Figure 12. Representative isotherm contours at $Re = 1$ (flow is from left to right).

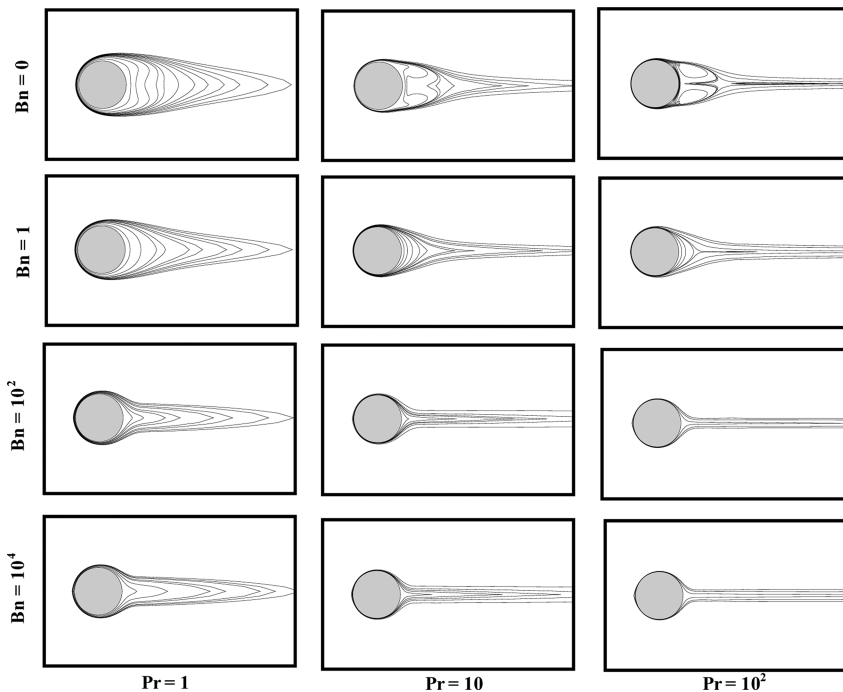


Figure 13. Representative isotherm contours at $Re = 100$ (flow is from left to right).

$$j_H = \frac{2.3}{Re^{*2/3}} \quad \text{for } 10^{-4} \leq Re^* \leq 0.199 \quad (28)$$

$$j_H = \frac{2.27}{Re^*} \quad \text{for } 0.199 \leq Re^* \leq 100 \quad (29)$$

while the overall resulting mean and maximum deviations are 14% and 35.5% in eq 28 and 18% and 40.32% in eq 29, respectively.

Before leaving this section, it is worthwhile to revisit the key assumptions inherent in the heat transfer results reported

herein. Perhaps the most severe assumption is that of constant thermo-physical properties. Among all the relevant properties, undoubtedly the Bingham plastic viscosity (μ_B) and yield stress (τ_0) are the most temperature-sensitive. For a common yield stress fluid used in the literature (Carbopol solution) Nouar and co-workers^{49,50} show that the yield stress appears to remain approximately constant across a rather large temperature range (10–85 °C), whereas the consistency index in the Herschel–Bulkley model exhibits a slight monotonic decrease with increasing temperature. In contrast a recent study by Weber et al.,⁵¹ for nominally the same Carbopol gel, reports that the

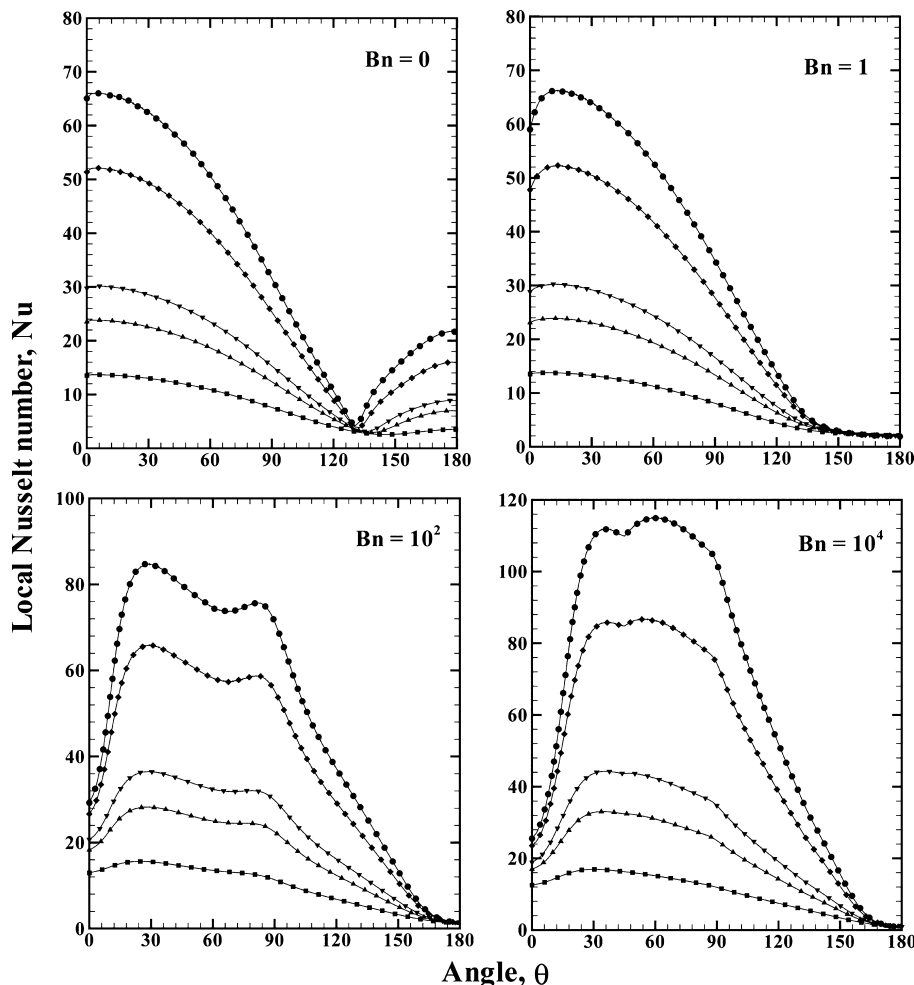


Figure 14. Variation of the local Nusselt number, Nu along the surface of sphere at $Re = 100$ (where $\theta = 0$ is the front stagnation point).

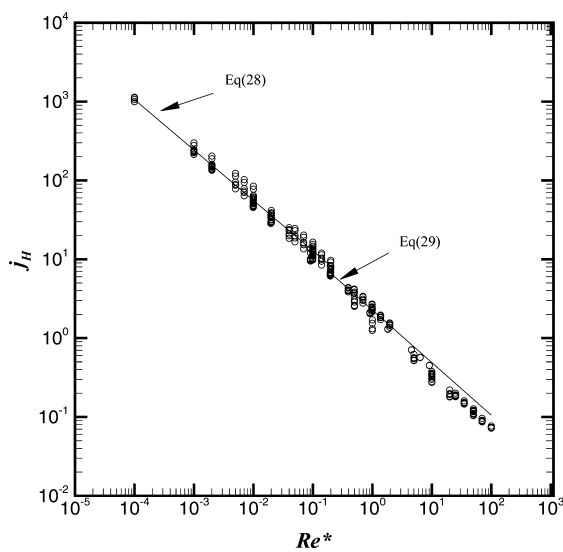


Figure 15. Dependence of the j -factor on the modified Reynolds number.

consistency index remains approximately constant, whereas the yield stress exhibits a complex nonmonotonic variation with temperature. In principle, there is no conceptual difficulty in incorporating such complex features in the analysis, albeit this will lead to coupling between the velocity and temperature

fields and one will thus have to solve them simultaneously as opposed to the sequential solution obtained in the present study. Given that there is still debate about even the qualitative nature of the effect of temperature on yield stress and consistency index/plastic viscosity, our current approach seems reasonable. Furthermore, as far as is known to us, very little data is available on the severity of the yield stress-temperature relationship of other fluids to develop universally valid forms of this functional relationship for arbitrary materials. Future studies in this field will hopefully address this and other pertinent issues.

5. CONCLUSIONS

The momentum and forced convection heat transfer characteristics of a heated sphere submerged in Bingham plastic fluids have been investigated numerically by using the exponential regularization scheme. Limited simulations were also performed by employing the biviscous model approach to corroborate the reliability of the present numerical results. Extensive results on detailed kinematics (streamline and isotherm contours, yielded/unyielded regions), surface pressure and the Nusselt number distribution over the surface of the sphere are studied over wide ranges of the pertinent parameters as $1 \leq Re \leq 100$, $1 \leq Pr \leq 100$, and $0 \leq Bn \leq 10^4$. The overall gross behavior is described in terms of the individual and total drag coefficient and Nusselt number. At the detailed level, the flow field in the proximity of the sphere consists of low and high shear zones.

Broadly, for a fixed value of the Reynolds number, the fluid-like (yielded) regions diminish with the increasing Bingham number, akin to the thinning of the boundary layers. This, in turn, sharpens the velocity and temperature gradients close to the surface of the sphere thereby enhancing the rate of heat transfer. The drag predictions at finite Reynolds numbers are found to be in agreement with the scant experimental results available in the literature. The present numerical values of drag coefficient and mean Nusselt number have been correlated with the modified definitions of the Reynolds number (Re^*), Prandtl number (Pr^*), and Bingham number (Bn^*). In the limiting case of Newtonian fluid behavior ($Bn = 0$), the values of drag and Nusselt number herein are found to be in line with the previous results.

AUTHOR INFORMATION

Corresponding Author

*Tel.: 0091 512 2597393. Fax: 0091 512 2590104. E-mail: chhabra@iitk.ac.in.

Notes

The authors declare no competing financial interest.

NOMENCLATURE

- Bn = Bingham number ($\equiv \tau_0 d / \mu_B V_0$), dimensionless
- Bn^* = modified Bingham number ($\equiv Bn / (1+Bn)$), dimensionless
- C_D = drag coefficient, dimensionless
- C_{DP} = pressure drag coefficient, dimensionless
- C = thermal heat capacity of fluid, $J \cdot kg^{-1} \cdot K^{-1}$
- C_p = pressure coefficient, dimensionless
- C_p^* = modified pressure coefficient ($C_p^* = C_p \times Re^*$), dimensionless
- C_s = Stokes' drag coefficient, dimensionless
- d = diameter of sphere, m
- F_D = drag force, N
- F_{DF} = frictional component of drag force, N
- F_{DP} = pressure component of drag force, N
- h = heat transfer coefficient, $W \cdot m^{-2} \cdot K^{-1}$
- H = lateral height of the domain, dimensionless
- k = thermal conductivity of fluid, $W \cdot m^{-1} \cdot K^{-1}$
- m = growth rate parameter, dimensionless
- n_s = unit normal vector on the surface of sphere, dimensionless
- Nu = local Nusselt number, dimensionless
- Nu_{avg} = average Nusselt number, dimensionless
- p = pressure, dimensionless
- P_0 = local pressure on the surface of sphere, Pa
- P_∞ = reference pressure far away from sphere, Pa
- Pr = Prandtl number ($\equiv C\mu_B/k$) dimensionless
- Pr^* = modified Prandtl number ($\equiv Pr(1+Bn)$), dimensionless
- R = radius of sphere, m
- Re = Reynolds number ($\equiv \rho dV_0 / \mu_B$), dimensionless
- Re^* = modified Reynolds number ($\equiv Re / (1+Bn)$), dimensionless
- S = surface area of sphere, m^2
- T = temperature of fluid, dimensionless
- T_w = sphere surface temperature, K
- T_0 = free stream fluid temperature, K
- V = velocity vector, dimensionless
- V_0 = uniform inlet velocity, $m \cdot s^{-1}$
- V_r = velocity component in r -direction, dimensionless

V_z = velocity component in z -direction, dimensionless
 r, z = cylindrical coordinates, dimensionless

Greek Symbols

- $\dot{\gamma}$ = rate of strain tensor, dimensionless
- $|\dot{\gamma}|$ = magnitude of the rate of strain tensor, dimensionless
- η = apparent viscosity, $Pa \cdot s$
- θ = position on the surface of sphere, deg
- μ_B = plastic viscosity, $Pa \cdot s$
- μ_y = yield viscosity, $Pa \cdot s$
- ρ = density of the fluid, $kg \cdot m^{-3}$
- τ = extra stress tensor, dimensionless
- τ_0 = yield stress, Pa
- $|\tau|$ = magnitude of the extra stress tensor, dimensionless
- ∇ = del operator, m^{-1}

Subscripts

- 0 = free stream or inlet condition
- w = sphere surface condition

REFERENCES

- (1) Walters, K.; Tanner, R. I. The motion of a sphere through an elastic liquid. In *Transport Processes in Bubbles, Drops, and Particles*; Chhabra, R. P., DeKee, D., Eds.; Hemisphere: New York, 1992; pp 73–86.
- (2) McKinley, G. H. Steady and transient motion of spherical particles in viscoelastic liquids. In *Transport Processes in Bubbles, Drops and Particles*; Chhabra, R. P., DeKee, D., Eds.; Taylor & Francis: New York, 2002; pp 338–375.
- (3) Chhabra, R. P. *Bubbles, Drops, and Particles in Non-Newtonian Fluids*, 2nd ed.; CRC Press: Boca Raton, 2006.
- (4) Chhabra, R. P.; Richardson, J. F. *Non-Newtonian Flow and Applied Rheology: Engineering Applications*, 2nd ed.; Butterworth-Heinemann: Oxford, 2008.
- (5) Suresh, K.; Kannan, A. Effect of particle diameter and position on hydrodynamics around a confined sphere. *Ind. Eng. Chem. Res.* **2011**, *50*, 13137–13160.
- (6) Suresh, K.; Kannan, A. Effect of particle blockage and eccentricity in location on the non-Newtonian fluid hydrodynamic around a sphere. *Ind. Eng. Chem. Res.* **2012**, *51*, 14867–14883.
- (7) Acrivos, A.; Shah, M. J.; Petersen, E. E. Momentum and heat transfer in laminar boundary layer flows of non-Newtonian fluids past external surfaces. *AIChE J.* **1960**, *6*, 312–317.
- (8) Acrivos, A. A theoretical analysis of laminar natural convection heat transfer to non-Newtonian fluids. *AIChE J.* **1960**, *6*, 584–590.
- (9) Dhole, S. D.; Chhabra, R. P.; Eswaran, V. Forced convection heat transfer from a sphere to non-Newtonian power-law fluids. *AIChE J.* **2006**, *52*, 3658–3667.
- (10) Song, D.; Gupta, R. K.; Chhabra, R. P. Effect of blockage on heat transfer from a sphere in power-law fluids. *Ind. Eng. Chem. Res.* **2010**, *49*, 3849–3861.
- (11) Song, D.; Gupta, R. K.; Chhabra, R. P. Heat transfer to a sphere in tube flow of power-law liquids. *Int. J. Heat Mass Transfer* **2012**, *55*, 2110–2121.
- (12) Prashanna, A.; Chhabra, R. P. Free convection in power-law fluids from a heated sphere. *Chem. Eng. Sci.* **2010**, *65*, 6190–6205.
- (13) Nirmalkar, N.; Chhabra, R. P. Mixed convection from a heated sphere in power-law fluids. *Chem. Eng. Sci.* **2013**, *89*, 49–71.
- (14) Bird, R. B.; Dai, G. C.; Yarusso, B. J. The rheology and flow of viscoplastic materials. *Rev. Chem. Eng.* **1983**, *1*, 1–70.
- (15) Barnes, H. A.; Walters, K. The yield stress myth? *Rheol. Acta* **1985**, *24*, 323–326.
- (16) Barnes, H. A. The yield stress—A review or “πανταρεῖ”—everything flows? *J. Non-Newt. Fluid Mech.* **1999**, *81*, 133–178.
- (17) Papanastasiou, T. C. Flow of materials with yield. *J. Rheol.* **1987**, *31*, 385–404.
- (18) Glowinski, R.; Wachs, A. On the numerical simulation of viscoplastic fluid flow. In *Handbook of Numerical Analysis*; Ciarlet, P. G. Ed.; Elsevier: North-Holland, 2011; pp 483–717.

- (19) Valentik, L.; Whitmore, R. L. The terminal velocity of spheres in Bingham plastics. *Br. J. Appl. Phys.* **1965**, *16*, 1197–1203.
- (20) Ansley, R. W.; Smith, T. N. Motion of spherical particles in a Bingham plastic. *AIChE J.* **1965**, *13*, 1193–1196.
- (21) Pazwash, H.; Robertson, J. M. Forces on bodies in Bingham fluids. *J. Hydraulic Res.* **1975**, *13*, 35–55.
- (22) Atapattu, D. D.; Chhabra, R. P.; Uhlherr, P. H. T. Wall effect for spheres falling at small Reynolds number in a viscoplastic medium. *J. Non-Newt. Fluid Mech.* **1990**, *38*, 31–42.
- (23) Atapattu, D. D.; Chhabra, R. P.; Uhlherr, P. H. T. Creeping sphere motion in Herschel-Bulkley fluids: flow field and drag. *J. Non-Newt. Fluid Mech.* **1995**, *59*, 245–265.
- (24) Hariharaputhiran, M.; Shankar Subramanian, R.; Campbell, G. A.; Chhabra, R. P. The settling of spheres in a viscoplastic medium. *J. Non-Newt. Fluid Mech.* **1998**, *79*, 87–97.
- (25) Horsley, M. R.; Horsley, R. R.; Wilson, K. C.; Jones, R. L. Non-Newtonian effects on falling velocities of pairs of vertically aligned spheres. *J. Non-Newt. Fluid Mech.* **2004**, *124*, 147–152.
- (26) Chafe, N. P.; de Bruyn, J. R. Drag and relaxation in a bentonite clay suspension. *J. Non-Newt. Fluid Mech.* **2005**, *131*, 44–52.
- (27) Beris, A. N.; Tsamopoulos, J. A.; Armstrong, R. C.; Brown, R. A. Creeping motion of a sphere through a Bingham plastic. *J. Fluid Mech.* **1985**, *158*, 219–244.
- (28) Bercovier, M.; Engelman, M. A finite element method for incompressible non-Newtonian flows. *J. Comput. Phys.* **1980**, *36*, 313–326.
- (29) Blackery, J.; Mitsoulis, E. Creeping motion of a sphere in tubes filled with a Bingham plastic material. *J. Non-Newt. Fluid Mech.* **1997**, *70*, 59–77.
- (30) Beaulne, M.; Mitsoulis, E. Creeping motion of a sphere in tubes filled with Herschel-Bulkley fluids. *J. Non-Newt. Fluid Mech.* **1997**, *72*, 55–71.
- (31) Prashant, J.; Derksen, J. Direct simulations of spherical particle motion in Bingham liquids. *Comput. Chem. Eng.* **2011**, *35*, 1200–1214.
- (32) Putz, A.; Frigaard, I. A. Creeping flow around particles in a Bingham fluid. *J. Non-Newt. Fluid Mech.* **2010**, *165*, 263–280.
- (33) Putz, A. M.; Burghelea, T. I.; Frigaard, I. A.; Martinez, D. M. Settling of an isolated spherical particle in a yield stress shear thinning fluid. *Phys. Fluids* **2008**, *20*, 033102–033113.
- (34) Jossic, L.; Magnin, A. Drag and stability of objects in a yield stress fluid. *AIChE J.* **2001**, *47*, 2666–2672.
- (35) Jossic, L.; Magnin, A. Drag of an isolated cylinder and interactions between two cylinders in yield stress fluids. *J. Non-Newt. Fluid Mech.* **2009**, *164*, 9–16.
- (36) Tokpavi, D. L.; Jay, P.; Magnin, A. Interaction between two circular cylinders in slow flow of Bingham viscoplastic fluid. *J. Non-Newt. Fluid Mech.* **2009**, *157*, 175–187.
- (37) Liu, B. T.; Muller, S. J.; Denn, M. M. Convergence of a regularisation method for creeping flow of a Bingham material about a rigid sphere. *J. Non-Newt. Fluid Mech.* **2002**, *102*, 179–191.
- (38) Frigaard, I. A.; Nouar, C. On the usage of viscosity regularisation methods for visco-plastic fluid flow computation. *J. Non-Newt. Fluid Mech.* **2005**, *127*, 1–26.
- (39) O'Donovan, E. J.; Tanner, R. I. Numerical study of the Bingham squeeze film problem. *J. Non-Newt. Fluid Mech.* **1984**, *15*, 75–83.
- (40) Nirmalkar, N.; Chhabra, R. P.; Poole, R. J. Laminar forced convection heat transfer from a heated square cylinder in a Bingham plastic fluid. *Int. J. Heat Mass Transfer* **2013**, *56*, 625–639.
- (41) Mitsoulis, E.; Zisis, T. H. Flow of Bingham plastics in a lid-driven square cavity. *J. Non-Newt. Fluid Mech.* **2001**, *101*, 173–180.
- (42) Nirmalkar, N.; Chhabra, R. P.; Poole, R. J. On creeping flow of a Bingham plastic fluid past a square cylinder. *J. Non-Newt. Fluid Mech.* **2012**, *171*–*172*, 17–30.
- (43) Sairamu, M.; Nirmalkar, N.; Chhabra, R. P. Natural convection from a circular cylinder in confined Bingham plastic fluids. *Int. J. Heat Mass Transfer* **2013**, *60*, 567–581.
- (44) Masliyah, J. H. Steady wakes behind oblate spheroids: Flow visualization. *Phys. Fluids* **1972**, *15*, 1144–1146.
- (45) Oh, J. H.; Lee, S. J. A study on the Newtonian fluid flow past a sphere in a tube. *Korean J. Chem. Eng.* **1988**, *5*, 190–196.
- (46) Nakamura, I. Steady wake behind a sphere. *Phys. Fluids* **1976**, *19*, 5–9.
- (47) Mossaz, S.; Jay, P.; Magnin, A. Criteria for the appearance of recirculating and non-stationary regimes behind a cylinder in a viscoplastic fluid. *J. Non-Newt. Fluid Mech.* **2010**, *165*, 1525–1535.
- (48) Uhlherr, P. H. T.; Park, K. H.; Tiw, C.; Andrews, J. R. G. Yield stress from fluid behaviour on an inclined plane. Proceedings of the Xth International Congress on Rheology, Acapulco, 1984, 183.
- (49) Nouar, C.; Desaubry, C.; Zenaidi, H. Numerical and experimental investigation of thermal convection for a thermo-dependent Herschel-Bulkley fluid in an annular duct with rotating inner cylinder. *Eur. J. Mech. B, Fluids* **1998**, *17*, 875–900.
- (50) Peixinho, J.; Desaubry, C.; Lebouche, M. Heat transfer of a non-Newtonian fluid (Carbopol aqueous solution) in transitional pipe flow. *Int. J. Heat Mass Transfer* **2008**, *51*, 198–209.
- (51) Weber, E.; Moyers-González, M.; Burghelea, T. I. Thermo-rheological properties of a Carbopol gel under shear. *J. Non-Newt. Fluid Mech.* **2012**, *183*–*184*, 14–24.